I certify that all material in this thesis that is not my own work has been identified and that no material has been included for which a degree has previously been conferred on me.

Signed……...

*Experimental Analysis of Forced and Confined Vortices for Varying Outlet Geometries*

**RUSSELL VENN**

**2011**

# 1 - Abstract

To validate and confirm results which have been obtained through computational fluid dynamic analysis for the introduction of outlets with three different geometries: circular (control), square and triangular; which have the availability of examining effects on complex situations, and under true in situ conditions; work was undertaken to directly compare the data obtained through experimental and computational methods through the utilisation of a simplified test rig. Using flow monitoring methods: pressure testing of the wall and base areas, flow velocity measurement using particle image velocimetry at varying heights, and visual inspection, for a range of flow rates; which were available to be analysed through computational methods, a general profile was deduced for each outlet geometry and these profiles were compared directly to determine the effect on the flow regions within the simplified rig, and therefore on the rotating motion in general, and also compared with the gathered computational results. It was determined that the circular outlet produces the highest vortex strength which results in higher core velocities and lower main flow velocities, and the triangular outlet displayed the lowest strength and the highest main flow velocities and pressures. Computational comparison highlights issues with the method of data capture utilised on the experimental rig and evident is the inability to detect high velocity gradients in small regions due to the sampling method and the data recording rate. A large pressure variation was found between computational and experimental methods and further work is advised to determine the primary cause for this discrepancy.

# 2 - Contents

# List of Figures



# List of Tables

# 3 - Project Description

The group project [Evolutions in Vortex Flow Control Design] is focused on improving the design of vortex flow control (VFC) devices through manipulation of the geometries within the device outlets. The group consists of eight members (four mechanical and four civil engineers), and the project has been separated into three distinct sections; computational, experimental and urban drainage:

As part of the experimental group section, this report focuses on the properties of vortices themselves; through testing of a basic rig with an outlet orifice plate which can be modified with various orifice geometries and has a variable flow rate. This gives an understanding of the differences in flow patterns and the variation in characteristic curve achieved with the proposed modifications. This is undertaken through visual inspection with the use of dye tracers to observe the flow patterns, with the application of particle image velocimetry (PIV) analysis; to produce velocity profiles of the flow for varying inlet flow rates, and through pressure testing of the fluid domain.

The experimental data produced using the test rig can be compared with simulations run using computational fluid dynamics (CFD) on a replicated situation. The validation of the results obtained in these CFD experiments is then used to justify results obtained for CFD simulations of other domain dimensions and orientations; where other members of the CFD group are focused on modelling the flow in a current VFC device, utilising the modifications being proposed by the project. The experimental group also undertook a general study of vortices; their formation and features of their flow, and looks into the characteristic flow of a VFC, including the critical point where simple flow coexists with a forming vortex, and the formation of a vortex thereafter.

# 4 - Background Information

## 4.1 - Hydro International

This project was undertaken with the backing and support of a multinational water management company who currently produce a range of products which utilise vortex flow to control the flow of fluids over a range of flow rates to aid in flood water management.

Hydro International Ltd is a medium sized limited company set up in 1982 (previously trading as Ouststar Ltd) with a workforce of 130 across several countries, who specialise in water management technologies, particularly waste and storm-water control. A large part of their storm-water solutions is the VFC device; known in the company as a HydroBrake. These have been implemented in locations with various storm water flow profiles, and details of two case studies; in Northampton and Leicestershire, demonstrate the scale of the solutions that can be installed.

The group has been in regular contact with a Hydro International employee (Mr Daniel Jarman) who is part of the engineering team working on water management devices. His previous research into computational studies on vortices has been available and his guidance has been given in depth to the CFD group.

Once the initial investigations were completed, the proposed modifications were tested further using Hydro International's test facility in North Somerset, where agreements were made to manufacture a new device which allowed for multiple outlet geometries to be attached at the rear and set up in the test facility to provide head vs. flow rate characteristic graphs for each outlet, which is then available to compare with the results obtained through CFD analysis.

# 4.2 - VFC Devices

Vortex flow control (VFC) devices: also known as vortex diodes and vortex brakes, are simple devices with an absence of movi7ng parts, designed to control fluid flow through a system by implementing a storage phase into a normal drainage system which occurs during high flow rate conditions (i.e., storm water periods).

The fluid enters the VFC perpendicular to the outlet orifice. During high flows this lateral velocity component creates a circular flow pattern that produces a vortex whose axis of rotation is situated along the axis of the outlet pipe. During this period of rotational flow, the discharge rate out of the orifice is significantly reduced such that an attached storage tank can be filled with the excess fluid. As the flow rate decreases at the ebb of the flood conditions, the vortex breaks down and the stored water flows through the outlet at a controlled rate. Once flow has returned to it's normal operating condition, the fluid enters the device in the same manner yet the flow velocity is not significant enough to produce any circular motion and the flow exits through the outlet orifice as if it were a standard pipe. This process provides an outlet discharge rate which remains close to the design point, so as to not overwhelm the system downstream of the VFC.

With increasing urbanisation of land creating greater water capacity requirements: particularly surface run-off during severe weather events, solutions to large volume flows over short time periods, which can also be utilised during normal conditions, are sought after, particularly if they can be implemented alongside pre-existing infrastructure and have a low installation and maintenance cost.

The production of a vortex at a certain value of pressure head produces a characteristic curve of flow rate with a distinct 'kickback' region where, the flow is significantly reduced for a minor head increase, and this initiates the storage phase of operation. The flow patterns either side of this transition phase are known to an extent, however the transition phase in particular is largely unknown. In general, VFC devices are designed to produce as high a gradient as possible for the phase 2 (rotational) flow and to have a kickback or transition phase with a high negative gradient.

# 5 - Proposed Modifications

The main aim of the project is to investigate the effect of utilising outlet orifices of varying geometries. The proposal is that, an outlet with a non circular orifice, which contains the same area as a relative circular orifice, will provide a more restricted outlet flow rate under high (or flood) conditions; which will theoretically alter the kickback section of the head vs. flow rate graph to produce a higher gradient, providing a more continuous flow profile; the ultimate aim of a VFC device.

There will be three different geometries tested. The benchmark orifice is circular and currently used on all Hydro International VFC devices, and this will be used as a comparison for the modified outlets, which are of square and triangle geometry, and each of these will be oriented in two directions, since the phase 1 flow is expected to be heavily dependant on the shape of the outlet.

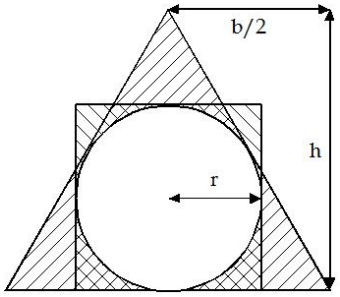


*Fig.1 - Overlaid geometries for different orifices, with retained circular geometry.*

The modified outlets may be investigated in two ways: firstly, that the area of the outlet remains constant, and the dimensions of the square and triangular shapes are reduced in order to achieve the area required. Alternatively, if it is assumed that the vortex which can be produced by an outlet, is only as large as the size of the circular shape that can be contained within it, then that basic circular dimension can be maintained and the square and triangular outlets will provide a higher area for the same size vortex, which may produce higher flow

rates under phase 1 flow. This situation is demonstrated in Fig.1, with the geometries overlaid to demonstrate the area benefit of the square and triangle.

$$Area_{\text{Circle}} = \pi r^2 = \pi 0.015^2$$

$$= 0.000707\, m^2$$

$$Area_{\text{Square}} = (2\text{r})^2 = 0.03^2$$

$$= 0.0009\, m^2$$

$$Area_{\text{Triangle}} = \frac{1}{2} bh$$

$$h = r + \frac{r}{\tan(30)}, \qquad b = \frac{2\text{r}}{\sin(30)}$$

$$Area_{\text{Triangle}} = \frac{r^2}{\sin(30)\tan(30)} + \frac{r^2}{\sin(30)}$$

$$= 0.00123\, m^2$$

$$Area\ Gain_{\text{Square}} = \frac{A_{\text{Square}}}{A_{\text{Circle}}} = \frac{0.0009}{0.000707} = 1.273$$

$$= 27.3$$

$$Area\ Gain_{\text{Triangle}} = \frac{A_{\text{Triangle}}}{A_{\text{Circle}}} = \frac{0.00123}{0.000707} = 1.740$$

$$= 74.0$$

## 5.1 - Project Aims

As part of the experimental section of the overall project tasked with investigating the use of different geometric outlets within a VFC device, this report aims to investigate the general flow patterns associated with different geometric outlets through the use of a purpose built test rig and to note the variations seen between the different types of outlet at varying flow rates. Alongside this, results will be obtained from the test rig with the aim of a comparison with CFD simulation results for an identical domain and under identical conditions to validate any results found using CFD for other simulated situations, to provide weighting to conclusions found regarding modifications to commercial parts, such as those produced by Hydro International.

# 6 - Evaluation Methods

As a VFC device inherently operates under two flow conditions: and these are substantially different in flow characteristics, they will be viewed as completely independent situations, and the very complex transition phase will not be considered in the 'in house' testing regime.

The testing undertaken within this section has been completed on a purpose build test rig manufactured by: and according to, [Newton (2011)] and is a vertically mounted part constructed of perspex, with the dimensions detailed in Fig.2. The test rig is connected directly to a pump powered water feed with a maximum flow rate of approximately 1.5 litres per second. A gate valve situated at the connection allows variation of the inlet flow rate, and the outlet is directed into a large diameter pipe, where no direct connection existed between the outlet orifice and the downstream pipe, therefore no downstream pressure issues could arise to affect the vortex flow.

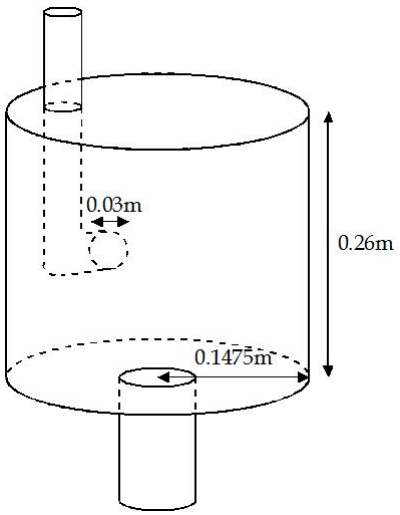


*Fig.2 - Basic inside dimensions of test rig.*

The outlet itself is contained within a small plate which sits in place within the base of the rig and can be removed and changed where necessary. Three outlet plates were therefore

produced with: circular, triangular and square sections.

Of the two methods of testing the various outlet geometries; as detailed in section 5; a constant outlet area has been utilised. This is primarily to maintain continuity with the computational group who are utilising an inlet to outlet ratio of 1:1, replicating the previous studies of [Jarman (2011)].

## 6.1 - Phase 1 Flow

This section of the flow; designed to run with inlet flow rates below the design point of the individual device; involves non-cyclical motion and is entirely based on fluid being drained out of the orifice at the rear of the device, with no vortex being present.

As the test rig is mounted such that the outlet is at the base of the system; providing a vertical axis to the vortex flow; the outflow under low flow rate conditions is purely vertical. This is distinct from the standard operating conditions of VFC devices, where a minimum fluid level is required prior to outflow occurring, as it must reac the lowest point of the outlet; centred at the mid point of the device. As such, outflow exists under all flow rates and experimentation is undertaken to determine the effect the geometry of the outlet has on the outflow rate. By finding the time taken to completely drain the tank, due to the constant outlet, any change in this drainage time can be linked to geometric differences.

## 6.2 - Phase 2 Flow

Three methods that can be utilised to monitor and review the flow within the rotational phase of the VFC can be used on the 'in house' test rig. By taking pressure readings at locations along the walls of the test rig, a profile of wall pressure can be found. Pressure readings taken at varying inlet flow rates can be compared for each of the outlet geometries to define any variation in the flow characteristics, and these pressure values are easily compared with results found through CFD simulation of identical situations.

Particle image velocimetry (PIV) is a method of flow analysis whereby a series of high

frequency images of the flow are captured by a camera; mounted perpendicular to the flow plane which is being studied; and particles: either objects already within the fluid or physically introduced (typically aluminium with a diameter of around 50μm), are mapped between locations on adjacent captured images. As the time between image capture is known, as well as the distance the particle has travelled over this time (this distance beling relative, where a scaling factor must be known to determine true distance), the particle can be assigned vector values for each image. By utilising a laser with a planar spread (this provides a sheet of light, as opposed to a beam, or 3D spread) positioned along the plane to be studied, and reducing the ambient lighting, the camera will only detect particles which exist in the plane, and therefore flow can be segmented to provide more directed analysis.

Using this technique, with a laser producing a plane which cuts through the entire domain, perpendicular to the axis of the vortex, will produce velocity vectors for the flow. These can be produced for a number of different locations within the domain, and for a range of flow rates for each outlet geometry. Production of velocity profiles of the flow may then be compared between the outlets to determine the effect of the outlet on the flow velocity within the test rig and therefore the effect on the vortex contained within it.

This method also allows for measurement of other flow characteristics, such as vorticity of flow (rate of rotation within a fluid) and turbulence intensity, and provides a time averaging ability to provide generalised flow characteristics.

# 7 - Phase 1

For this phase of flow, the outlet can be seen to act as either: a simple orifice; with a flow rate and pressure head relationship, or as a weir with flow characteristics dictated by the fluid height and the geometry of the weir section. In general, where the fluid level is at least at the lowest point of the outlet, and below the maximum outlet height, and where the outlet flow rate is adequate to retain a relatively stable situation, the weir flow characteristics prevail.

Where the fluid level raises to a point where the outlet is dimensionally small in relation to the height of the fluid flowing through it, where there is a negligible change in pressure over the height of the outlet and a negligible volumetric difference with variation in the level of the fluid, the outlet can be seen to act as an orifice. The approximations for orifice flow rely on the pressure head of the fluid above it.

## 7.1 - Weir Flow

Since the geometry of the orifice differs from the geometry of the outflow pipework attached immediately after the VFC, it is appropriate to model the orifice as a thin plate as opposed to a broad crested weir. These have a characteristic profile which is rarely knife-edged but has a small thickness and angled trailing edge.

To predict the flow patterns of the three orifice options being studied, their geometries are being modelled as weirs of different types and geometries. With weirs, care must be taken to ensure that effects of the flow upstream of the device are not significant to the downstream flow. In particular attention must be paid to wall effects. Since the distance between the edges of the VFC and the edges of the orifice are significant, the side contractions can be considered 'fully developed'. This is to say that the sides of the tank do not interfere with the side contractions of the nape [Ackers et al. 1978].

There have been multiple attempts to define the flow rate over a thin plate weir with a rectangular cross section, all of which are based upon the Bernoulli equation.

$$\textit{At Point A:} \quad H_1 = \frac{P_1}{\rho g} + z_1 + \frac{u_1^2}{2g}, \quad \textit{If}: y_1 = z_1 + \frac{P_1}{\rho g}$$

$$H_1 = y_1 + \frac{u_1^2}{2g}$$

$$\textit{At Point B:} \qquad H_2 = z_2 + \frac{u_2^2}{2g}$$

*Assuming there are no losses, and $P_2$ is atmospheric.*

$$y_1+\frac{u_1^2}{2g}=z_2+\frac{u_2^2}{2g}$$

$$u_2^2=\left(y_1-z_2+\frac{u_1^2}{2g}\right)2g$$

$$u_2=\sqrt{2g\left[y_1-z_2+\frac{u_1^2}{2g}\right]}=\left(2g\left(y_1-z_2\right)+u_1^2\right)^{\frac{1}{2}}$$

Therefore, $u_2$ is a function of $y_1$ and $z_2$, and so varies with elevation over the weir. If the discharge at B is taken for an elemental strip of height $\delta z$, and width b:

$$\partial Q=u_2 b\partial z$$

$$\partial Q=\left(2g\left(y_1-z_2\right)+u_1^2\right)^{\frac{1}{2}} b\partial z$$

With the height of the streamline remaining constant (not a realistic assumption):

$$Q=\int_0^{h_1} u_2 b\partial z$$

*b is constant, and* $\frac{u_1^2}{2g}$ *is negligible compared with* $h_1$:

$$Q=\frac{2}{3}b\sqrt{2g}\,h_1^{\frac{3}{2}}$$

Due to the vena contracta over the weir, the height of the streamline decreases over the distance from A to B, and therefore Q is lower than predicted. A weir coefficient, $C_d$ must be defined to demonstrate the relationship $Q/Q_{Ideal}$.

$$Q=\frac{2}{3}c_d b\sqrt{2g}\,h_1^{\frac{3}{2}}$$

The Francis equation is commonly utilised and has imperial units. It considers flow where the upstream approach velocity is negligible and includes a term for the number of

contractions, where fully developed flow has a value of η = 2. It assumes that each contraction contributes a potential weir width loss which equates to 5% of the head.

$$Q_{Francis} = C_d (b - 0.1 \eta h_1) h_1^{3/2}$$

Here, the constant $C_d$ = 0.587, and the conversion must be made into imperial units, giving the following formula, however in reality, a constant coefficient is inadequate when proper account is taken of approach effects, or in any instance where $H_1/P_1$ is large.

$$Q_{Francis} = 3.33 \left(b - 0.1 \eta h_1\right) h_1^{\frac{3}{2}}$$

There are many more approximations made to consider the effect seen through contractions, the Hamilton-Smith approximation considers the upstream velocity:

$$Q_{Hamilton\text{-}Smith} = 0.581 (1 - 0.1 \frac{H_1'}{b}) b \sqrt{g} H_1'^{3/2}$$

*Where:*

$$H_1' = h_1 + 1.4 \frac{v_a^2}{2g}$$

This however, contains specific dimensional requirements, where $h_1/P_1$, and $h_1/b$ must be less than 0.5. and where both $P_1$ and b must be greater than 0.3m.

The Kindsvater-Carter approximation covers a wide range of possible $h_1/P_1$ values, from 0.1 to 2.5. For the dimension of $P_1$ on the test rig ($P_1$ = 0.1325), this provides a range of $h_1$ values of 0.01325 to 0.3313m, therefore providing a solution for a nearly submerged outlet.

$$Q_{\text{Kindsvater-Carter}} = C_e \dot{b}_e \dot{H}_e^{\frac{3}{2}}$$

$$C_e = 1.78 + 0.22 \frac{h_1}{P_1}$$

$$b_e = b + k_L \quad \text{and} \quad H_e = h_1 + k_h$$

Where, L is the weir length, and the constants $K_L$ and $K_H$, and the relationship $C_e$, are all obtained through experimental data.

$$K_H = 0.001\text{m}, \qquad K_L = -0.001\text{m}$$

$$Q_{Kindsvater\text{-}Carter} = \left(1.78 + 0.22\frac{h_1}{P_1}\right)(b - 0.001)\left(h_1 + 0.001\right)^{\frac{3}{2}}$$

These predictions for the flow rate out of a rectangular weir were considered for the test rig dimensions, giving:

$$Q_{Standard} = 0.08859\, h_1^{\frac{3}{2}}$$

$$Q_{Francis} = \left(0.3278 - 0.666\, h_1\right) h_1^{\frac{3}{2}}$$

$$Q_{Kindsvater\text{-}Carter} = \left(1.78 + 1.66\, h_1\right)(0.029)\left(h_1 - 0.001\right)^{\frac{3}{2}}$$

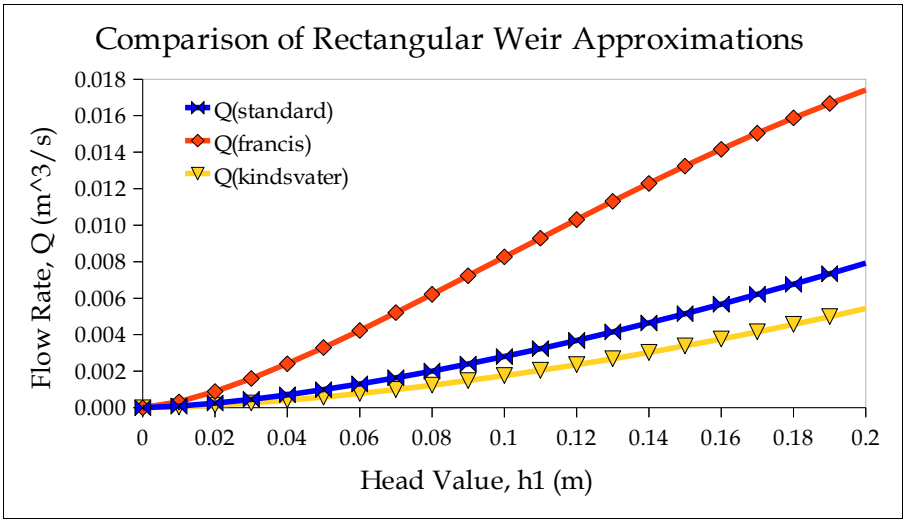


*Fig.3 - Rectangular weir flow rate approximations for test rig dimensions.*

For a triangular section outlet, a v-notch weir can be analysed. Similarly to the previous cases, the flow is split into a series of horizontal elements, with the local velocity at a given height being given by a potential energy.

$$Q = 2\sqrt{2}\tan\left(\frac{\theta}{2}\right)\sqrt{g}\left[\frac{4}{15}h_1^{\frac{5}{2}} + \frac{2}{5}\left(\frac{v_a}{2g_{\dot{c}}}\frac{5}{2}\right) - \frac{2}{3}h_1\left(\frac{v_a}{2g_{\dot{c}}}\frac{3}{2}\right)\right]\ldots$$

If the area of the upstream container is large; and therefore the approach velocity is negligible; and the discharge coefficient is incorporated to allow for the oversimplified theory then:

$$Q = \int \sqrt{2g}\, b\, h^{\frac{3}{2}} \;\partial h$$

*Where*

$$b = 2\tan\left(\frac{\theta}{2}\right) h_1$$

$$Q_{v\,notch} = \int_{h_1}^{0} 2\sqrt{2g}\tan\left(\frac{\theta}{2}\right) h^{\frac{3}{2}} \;\partial h$$

$$Q_{v\,notch} = C_d{}' \frac{4}{5}\tan\left(\frac{\theta}{2}\right)\sqrt{2g}\, h_1^{\frac{5}{2}}$$

In this instance $C_d{}'$ is found experimentally. Here the surface tension acting on the weir; at the nape; and the viscosity of the fluid are incorporated through the introduction of the effective head concept. The Kindsvater-Shen evaluation concludes that the discharge coefficient is dependant on the notch angle, and the respective values can be found through BS 3680. The orifice being evaluated and tested is equilateral and therefore has a 60 degree notch angle. Thus the coefficients:

$$\theta = 60$$

$$C_e = 0.576$$

$$k_v = 0.004\, ft \quad = 0.0012\text{m}$$

$$Q_{Shen} = C_e\, n \frac{4}{5}\tan\left(\frac{\theta}{2}\right)\sqrt{2g}\,(h_1 + k_v)^{\frac{5}{2}}$$

$$Q_{Shen} = 0.4608\tan(30)\sqrt{2g}\,(h_1 + 0.0012)^{\frac{5}{2}}$$

$$Q_{Shen} = 1.178\left(h_1 + 0.0012\right)^{\frac{5}{2}}$$

For a circular weir, the same principle applies, with the value of weir length being derived from the chord length for a given height, $h_1$.

$$Q = \int \sqrt{2g}\, b\, h^{\frac{3}{2}}\ \partial h$$

*Where*

$$b = 2\sqrt{r^2 - (r - h_1)^2}$$

$$Q_{circle} = 2\sqrt{2g} \int_{h_1}^{0} \sqrt{h_1}\left(0.015^2 - (h_1 - 0.015)^2\right)^{\frac{1}{2}}\ \partial h$$

The circular weir geometry was analysed numerically and compared with the averaged value of the three rectangular outlet approximations and the v notch approximation, as shown in Fig.4.

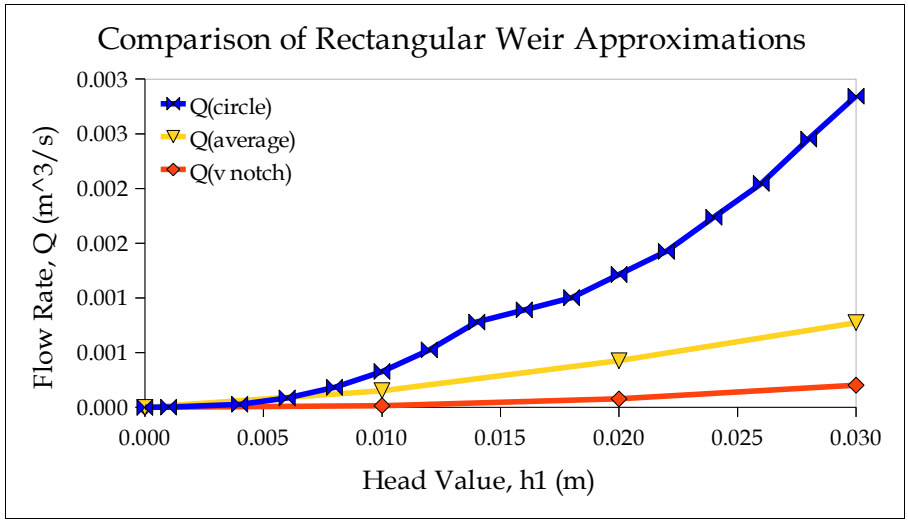


*Fig.4 - Comparison of three outlet flow approximations for weir flow.*

## 7.2 - Orifice Flow

To calculate the flow rate through an orifice, Bernoulli's principle is applied at the surface of the fluid above the orifice; which has a zero gauge pressure and a zero velocity; and just outside the orifice at the vena contracta, where the jet of fluid has a reduced diameter; where there is again zero gauge pressure.

$$Z_A + \frac{V_A^2}{2g} + \frac{P_A}{\rho g} = Z_B + \frac{V_B^2}{2g} + \frac{P_B}{\rho g}$$

$$Z_A - Z_B = H, \quad V_A = 0, \quad P_A = P_B = P_{ATM}$$

$$H = \frac{V_B^2}{2g}$$

$$V_B = \sqrt{2gH}$$

$$Q = VA = \sqrt{2gH}\, A$$

In a practical sense there is an energy loss throughout the system which can be incorporated by a coefficient $C_d$ which is approximately 0.97 for a circular outlet. The vena contracta also has an effect on the flow rate since it alters the area of the outlet fluid stream. This can be measured experimentally but can be considered approximately 0.64 for a sharp edge. This gives an overall coefficient of $C_d$=0.621.

If the orifice is first considered to adhere to the requirements of these formula, then the maximum flow rate for the outlet area used within the test rig; using a head value of 0.1475, which is the rig radius and therefore the maximum height of fluid above the centre of the orifice, is given by:

$$A = \pi r^2 = \pi 0.015^2 = 0.0007069\, m^2$$

$$Q_{orifice} = 0.621 \times 0.000707 \sqrt{2 \times 9.81 \times 0.1475}$$

$$Q_{orifice} = 0.000747\, m^3/s$$

If the orifice is considered large in comparison to the head of fluid flowing through it then there will be a substantially different head value at the top and bottom edges of the orifice and so the standard approximation is inadequate to describe the flow through it. As a result the flow is analysed as a series of horizontal elemental strips, as used in weir flow analysis.

*Area of Strip,* $A = B\,\delta\,h$

*Velocity of Flow through Strip:* $V = \sqrt{2gH}$

*Discharge through strip:* $Q = VA = B\sqrt{2Hg}\,\delta\,h$

*Total Discharge:* $Q_{orifice} = \sqrt{2g}\int_0^H B\,h^{\frac{1}{2}}\,\delta\,h$

$$B_{circle} = 2\sqrt{r^2-(r-h)^2}$$

$$Q_{circle} = 2\sqrt{2g}\int_0^H \sqrt{0.015^2-(0.015-h)^2}\sqrt{h}\,\delta\,h$$

$$B_{square} = r$$

$$Q_{square} = \sqrt{2g}\int_0^H 0.015\sqrt{h}\,\delta\,h$$

$$= 0.0443\,h^{\frac{3}{2}}$$

$$B_{triangle} = 2\tan\left(\frac{\theta}{2}\right)h$$

$$Q_{triangle} = 2\sqrt{2g}\tan(30)\int_0^H h\sqrt{h}\,\delta\,h$$

$$= 5.115\,h^{\frac{5}{2}}$$

## 7.3 - Vertical Flow

The test rig is designed to be mounted vertically, thus the weir and orifice calculations do not apply to the rig itself. The outlet instead acts as a sink hole and the flow is perpendicular to the free surface. With the area of the outlets all being equal, and the discharge flow rate being dependant on area and pressure of the fluid alone, the three outlets should be considered equal under low flow rates, with only the effect of the vena contracta; which will vary due to the outlet geometries; being significant in affecting the flow rate.

The equations found in sections 7.1 and 7.2 however, still apply to real VFC devices and therefore should be verified experimentally to determine the most accurate representative approximation of the flow.

# 7.4 - Drainage Period Measurement

To determine the coefficient of the vena contracta; and the geometric affect on the outlet flow; the three outlets were tested to find the time taken to discharge completely.

Theoretically, the outlet coefficient for a circular orifice is determined at $C_o = 0.6$. This gives a predicted drainage time of:

$$Q = C_o A_o \sqrt{2gH}$$

$$Q_{theoretical} = 0.6 \times 0.0007069 \sqrt{2gH}$$

$$= 0.001879 \sqrt{H}$$

*In $\delta t$ the height changes by $\delta H$,*

$$Q \delta t = -A \delta H$$

$$\frac{\delta t}{\delta H} = \frac{-A}{Q} = \frac{-A}{0.001879 \sqrt{H}}$$

$$t_{theoretical} = \int_0^{0.26} \frac{\pi 0.1475^2}{0.001879} H^{-0.5} \delta H$$

$$= 37.1 s$$

## *7.4.1 - Methodology*

For each of the three outlet geometries, the test rig was filled with water from the inlet pipe, and, at the point of the gate valve being closed, a timer was started. This was stopped when the velocity of the fluid in the tank became negligible (due to the construction of the tank, with a flat base, fluid was available to remain at the base, up to 2mm high). This was repeated three times, and the times averaged and then compared.

## 7.4.2 - Results

| | Drainage Time (s) |
|---|---|
| **Ideal** | 37.1 |
| **Circular** | 41.5 |
| **Square** | 43.2 |
| **Triangular** | 44 |

*Tab.1 - Drainage periods for three outlets located vertically.*

## 7.4.3 - Analysis

The drainage time for the three outlets are similar; however, there is a 6% difference between the minimum and maximum values; however all exceed the expected discharge time. A significant factor in this may be the gate valve used to stem the inlet flow. Since this is a screw valve which requires some five full rotations to completely stop the fluid inlet, there is a period at the start of the measured period where there is an imbalance, with an unknown input. To start the timings when the valve is completely closed however, would involve assuming that the inlet flow maintains the full capacity of fluid in the tank, up until the point at which it closes. Essentially, in either case, the valve is assumed to be a discrete input.

If the valve effect is assumed to be constant in all three cases, and the circle is taken as the ideal case, with a discharge coefficient of 0.6, then coefficients can be found for the square and triangular orifices.

$$t_r = t_i C_d C_g$$

$$\textit{assuming } C_g = 0 \textit{ for circle}, \quad C_d = \frac{41.5}{37.1} = 1.119$$

$$C_{g\,square} = \frac{t_r}{t_i C_d} = \frac{43.2}{37.1 \times 1.119} = 1.041$$

$$C_{g\,triangle} = \frac{t_r}{t_i C_d} = \frac{44}{37.1 \times 1.119} = 1.060$$

The theoretical discharge times, negating the inconsistency with closure of the valve, are then given as:

$$t_{square} = t_i C_g = 37.1 \times 1.041$$
$$= 38.6\, s$$

$$t_{triangle} = t_i C_g = 37.1 \times 1.06$$
$$= 39.3\, s$$

# 8 - Phase 2

For the experiments on the rotational flow within the test rig, an orifice plate was added to the inlet pipe with pressure gauges situated either side which were calibrated to known flow rates. The readings of these gauges, when compared, provide an accurate figure of the inlet flow rate, and with the calibration completed, the following relationships are used to determine the flow rates.

$$Q_T = A_2 \sqrt{\left[\frac{2(P_1 - P_2)}{\rho}\right] / \left[1 - \left(\frac{A_1}{A_2}\right)^2\right]}$$

$$Q_A = 18.705\, Q_T^3 - 2.9933\, Q_T^2 + 0.1711\, Q_T - 0.0028$$

*Where*

$$A_1 = 1.25\, inch, \qquad A_2 = 0.75\, inch$$
$$= 0.0318\, m, \qquad = 0.0191\, m$$

## 8.1 - Pressure Measurement

### *8.1.1 - Methodology*

A large, multi-tube manometer was connected up to a series of holes made in the base and side wall of the test rig, such that a flush edge was seen on the inside wall, and the

manometer connection tubes could be removed and the holes filled to ensure the fluid flow was not disturbed unnecessarily. The positions of these pressure tapping points is shown in Fig.5.

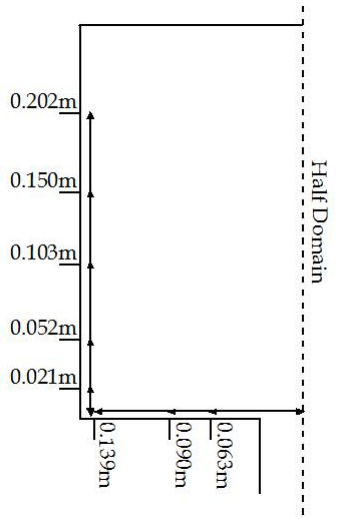


*Fig.5 - Locations of pressure reading positions (shown on half of the test rig).*

A datum level was found with the manometer placed a constant height above the free surface of the VFC, and the angle which the manometer was positioned at was recorded. By angling the manometer, the fluid in the tubes travels over a larger distance for equivalent pressure change, therefore a higher precision of recorded data is achievable.

For a range of flow rates from the formation of a vortex (the end of the transition phase) to the maximum flow rate available (approximately 1.5 L/s) the flow rate was varied and the values given by the two pressure gauges were noted at the point at which a clamp on the manometer was applied, giving a constant reading.

## *8.1.2 - Data Manipulation*

Initially, the pressure values found from the orifice plate were converted into Pascals, and the flow rate was found. The height of the fluid within the manometer was then calculated from the recorded values. This was done by multiplying the recorded value by a conversion factor (since the gauge was in inches) and converting this value into a vertical height. This being added to the height of the datum point. This height was then converted into a gauge pressure value through multiplication of the density of water (taken at $20^{o}C$ as 998.2 $kg/m^{3}$)

and by gravitational acceleration and this was converted into Pascals through division of 1000 (since measurements were taken from millimetres).

These values were also normalised by dividing each pressure value at each tapping position by the volumetric flow rate for that set of data points.

### *8.1.3 - Results*

The results of gauge pressure for a range of flow rates were plotted on two sets of graphs (one for the pressure tappings along the base of the rig, another for the pressure tappings up the side wall) for each outlet, giving the six graphs shown.

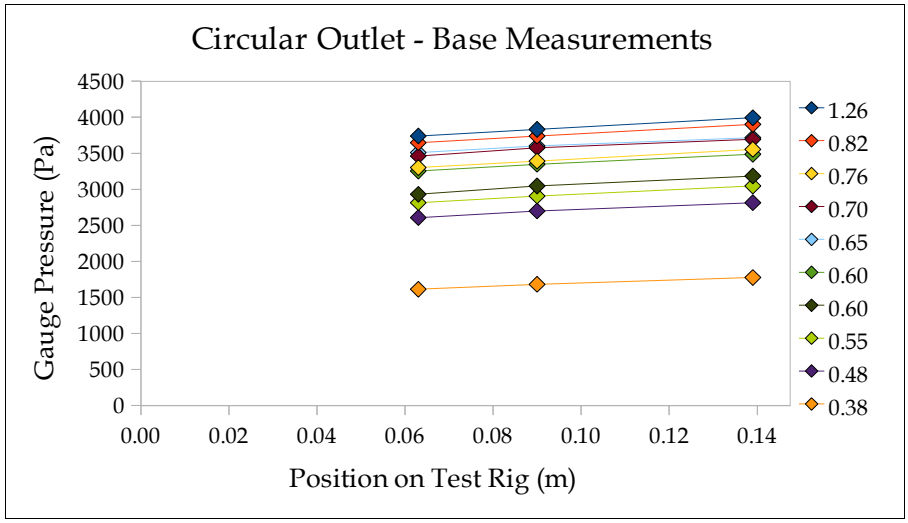


*Fig.6 - Base pressure measurements for circular outlet.*

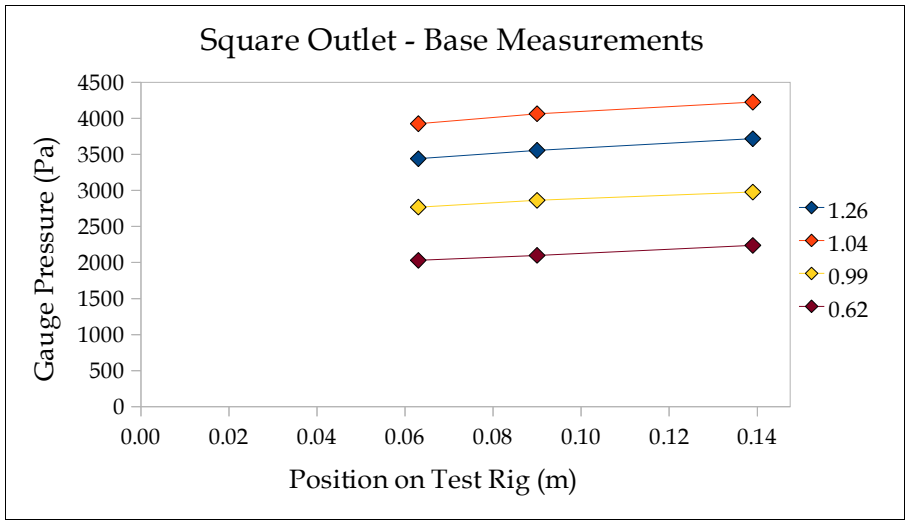


*Fig.7 - Base pressure measurements for square outlet.*

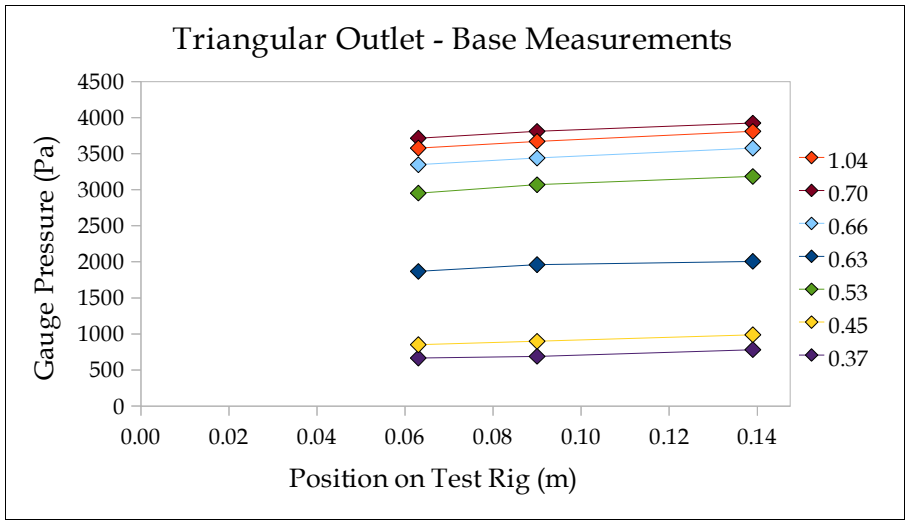


*Fig.8 - Base pressure measurements for triangular outlet.*

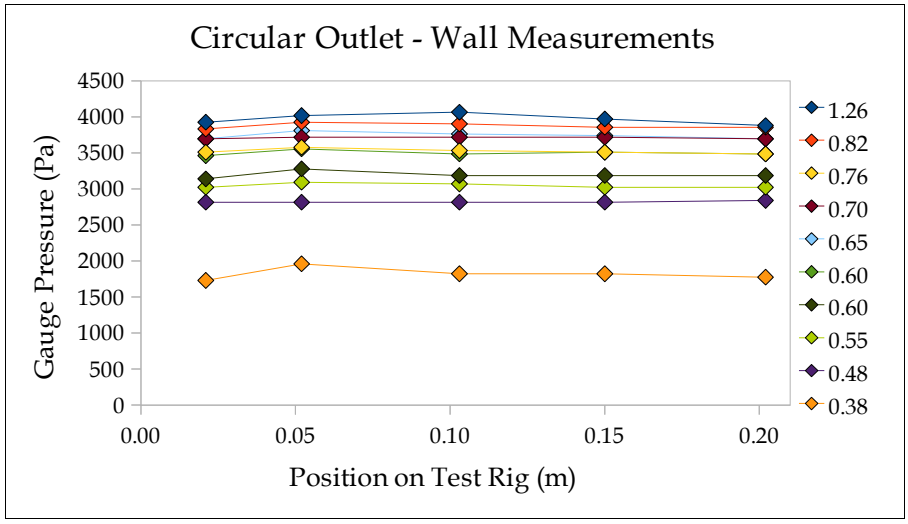


*Fig.9 - Wall pressure measurements for circular outlet.*

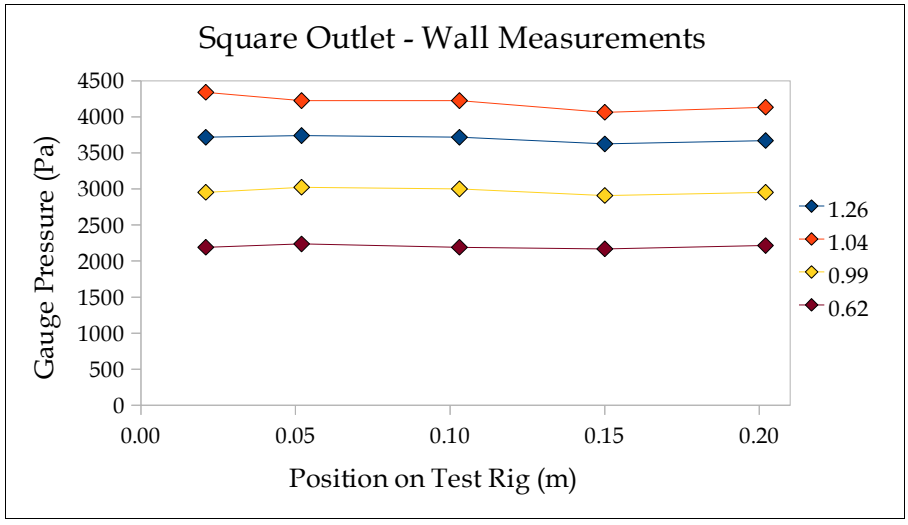


*Fig.10 - Wall pressure measurements for square outlet.*

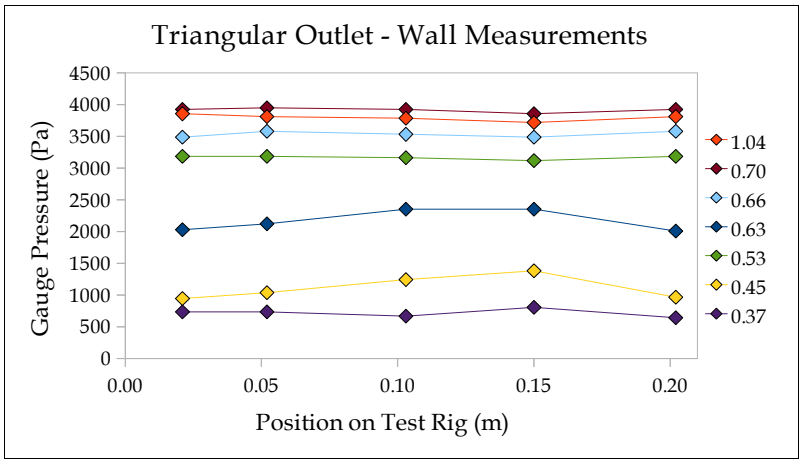


*Fig.11 - Wall pressure measurements for triangular outlet.*

The pressure readings along the wall for each flow rate were averaged and plotted against flow rate to demonstrate the general relationship between pressure and flow rate (Fig.12).

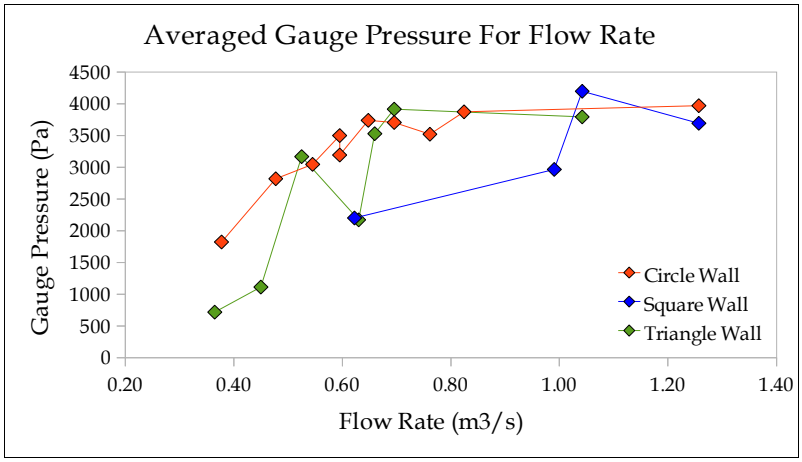


*Fig.12 - Pressure values averaged for each flow rate tested.*

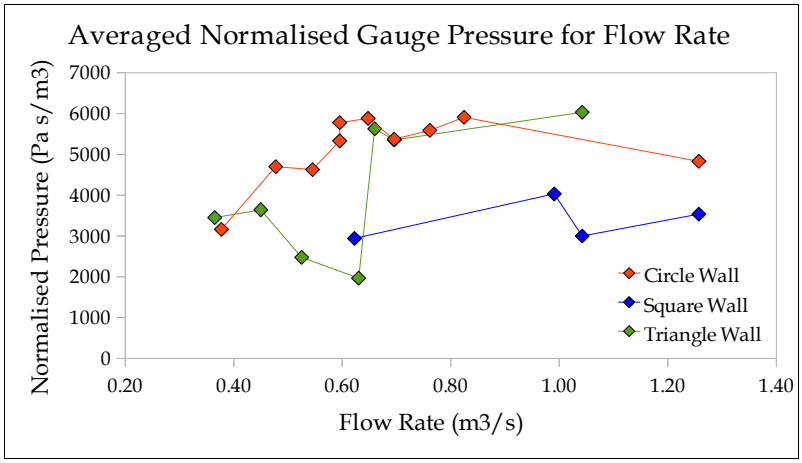


*Fig.13 - Pressure values normalised with inlet flow rate.*

## *8.1.4 - Analysis*

Application of Bernoulli's principle, to the flow gives the relationship between flow velocity; v, and pressure change; P.

$$\frac{P_1}{\rho g}+\frac{v_1^2}{2g}=\frac{P_2}{\rho g}+\frac{v_2^2}{2g}+\delta H$$

$$\delta P=\left(v_2^2-v_1^2\right)\rho$$

$$\delta v=\sqrt{\frac{\delta P}{\rho}}$$

When this relationship was applied to the flow rate into the test rig, the calculated pressure (not specific to a section of flow, since no area was included in the conversion from volumetric flow rate to velocity, and since the results are directly proportional regardless) was plotted alongside the recorded average pressure for the same flow rate (see Fig.14). With two anomalous results disregarded, there is a clear linear relationship between the calculated and recorded pressures, this demonstrates the VFC devices behaviour is subject to standard Bernoulli's principles. There is a difference however in the proportionality of the relationship, with the circular outlet having the highest measured pressure values, and the square section having the relationship nearest to 1:1. There is clearly a difference in the structure of the flow therefore, between the three outlets.

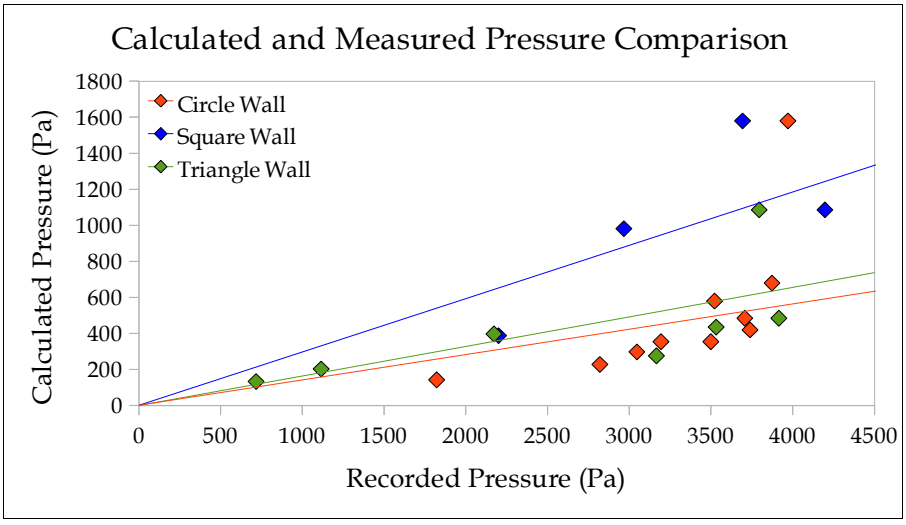


*Fig.14 - Comparative graph of recorded, and ideal pressure values.*

The six graphs (Fig.6 to Fig.11) demonstrate small, but noticeable variation in pressure over the test rig domain. From the base measurements, there is an obvious positive trend toward the wall, with an 8.4% and 11% variation over the measured area for the triangular and square, and the circular outlet. These would tend to indicate an increase in flow rate towards the wall as well; and since no reading was taken within the wall effect area of flow, this can generally be accepted, due to the direct proportionality between velocity and radial position (with a constant angular velocity).

The wall measurements demonstrate, for the most part, a quadratic relationship; with the highest pressure (and therefore velocity) being found within the mid section of the wall and in the main flow section, away from the base, and lid. Due to a vortex's structure, at the base of the main vortex, there is often a radial flow velocity towards the centre. This combined with the wall effect of the base, will reduce the overall velocity, and thus decrease the pressure. The same is true of the lid, however, since the vortex is forced, there is little radial velocity in this location, yet wall effects still contribute significantly.

In the averaged pressure graphs, the results for all three outlet geometries demonstrate an asymptotic relationship which results in a reduced $\delta P/\delta V$ as the flow rate increases. This is not predicted since the P/v relationship is quadratic, and therefore the differential is a linear relationship with velocity. However, since all three outlets demonstrate this relationship, and even when normalised, the trend is apparent, this can be taken either as a property of the flow, or as being unreliable data when averaged.

## 8.2 - Flow Velocity Measurement

### *8.2.1 - Methodology*

A PIV system was set up to monitor and record data from the test rig. This initially involved creating a large shield to reduce the ambient light level in the room, to produce higher quality feedback from the camera which was mounted approximately 1.5m above the test rig, with the full domain being visible.

The laser was positioned on a tripod approximately 1m away from the test rig, and with the

beam being maintained level throughout the experimentation, the laser was raised and lowered throughout the height of the rig, with measurements being taken at the positions detailed in Fig.15. For each of the three outlets, the flow rate was varied over its full range (from vortex formation up to the flow limit) and the PIV system was set to record data over a range of the heights shown.

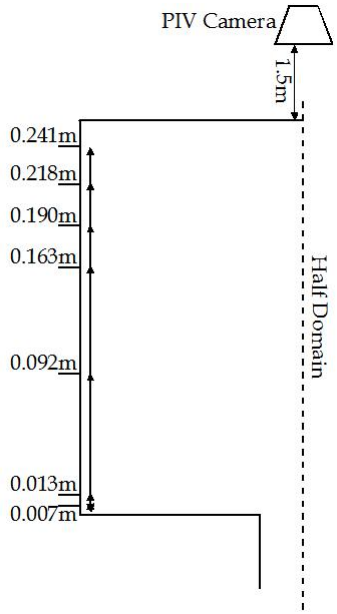


*Fig.15 - Locations of PIV laser positions (shown on half of the test rig).*

Again the flow rate was obtained from the orifice plate readouts, however since the PIV system can be set up to take readings over a period of time, these readings were averaged over time (since there is apparent variation over extended periods due to the discrete nature of the pump which feeds the water).

The camera was set to a frequency of 100Hz and readings of vectors for each coordinate in the domain were saved.

## *8.2.2 - Data Manipulation*

The PIV system output a .csv (comma separated variable) file for each time step recorded and this contains every coordinate within the visible domain of the camera. Where the laser is used, this only stores the test rig domain, since surrounding objects are not illuminated, and the particles in the air are not detected.

Two methods of data manipulation were undertaken, one which allowed for analysis of the tangential velocity components of a single sample line (an angle θ rad) over the range of radial distance from the centre point of the vortex to the side wall, and another which took an average of a number of data sets, then took the average value of tangential velocity for each 0.01m radial position, using the data from a large range of angles from the flow. For these two manipulation methods, the initialisation and results production were separate, however the data sorting and filtering was identical for both, this is detailed below.

Since an 8px (pixel) sample rate was used by the PIV system (a higher sample rate resulted in slower recording of data, and therefore a lower sample rate, which can result in the software not being able to track all the particles), the coordinates are stored every 8px. Using a stored image of the domain and discovering the side wall positions, the domain was found to exist from the coordinates (4,4) to (636,476). Interpolating between the reference positions on the image, and using a visual reference of the vortex to determine the axis of rotation, the x coordinate was found to be 5/17 between 350 and 400px, so existing at 364.7px, and the y coordinate at 3/17 between 250 and 300px, so existing at 258.8px. Since there are only coordinates situated every 8px, and the domain sample starts at 4, using:

$$\frac{(x-4)}{8} \equiv \mathbb{Z} \, \mathbb{R}$$

The coordinates of the centre point were found as (364,260).

To discover the coordinates of the radius of the test rig, two methods were employed: firstly an image was taken using the PIV system in an identical position, of a scaled ruler. Using this image, it was found that there are 54px/inch, and since 1 inch = 0.0254m, there are 2126px/m.

$$54\ px/inch$$

$$1\,inch = 0.0254\,m$$

$$2126\ px/m$$

Since the inside radius of the test rig is known, the length in px can be found:

$$r = 0.1475\,m$$

$$r = 0.1475 \times 2126\,px$$

$$= 313.585\,px$$

A second method involved using an image taken by PIV and finding a reference point on the inside edge of the rig. A point was chosen where the wall was visible and interpolation between the scaled reference points gave a coordinate of (580,120). Again, as the radius of the test rig is known, the px/m scaling factor was found:

$$r_{px} = \sqrt{(580-364)^2 + (120-260)^2}$$
$$= 257\,px$$

$$r_m = 0.1475\,m$$

$$\frac{px}{m} = \frac{257}{0.1475} = 1742\,px/m$$

There is clearly a large deviation between these two values; 1: 0.82, however for future reference, the lower value of 1742 px/m will be used.

To determine the flow over a radial spread from the centre point, an equation was produced to give the angle which any sampled coordinate makes with the centre point, and a horizontal line through the domain. Fig.16 demonstrates the positioning of this set up.

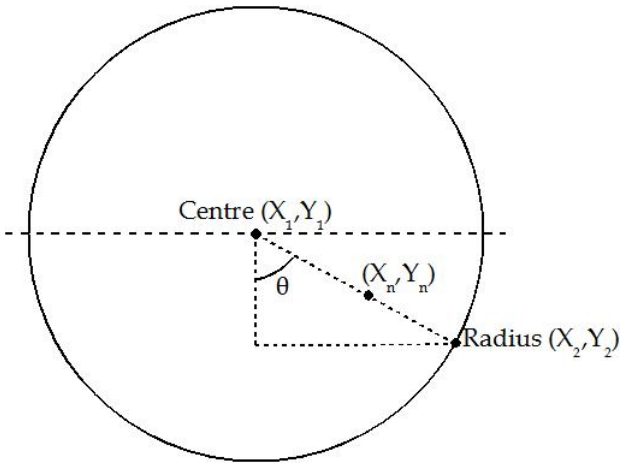


*Fig.16 - Coordinate positioning set up.*

$$\theta = \tan^{-1}\left(\frac{x_n - x_1}{y_n - y_1}\right)$$

Visual inspection of the images provided guidance on particular areas of flow. It is evident that part of the inlet pipe is visible in the recorded data, and this is due to it's proximity requirements which were unavoidable. This rendered the results for a portion of the domain inapplicable to analysis, since the PIV system detected the movement of the water flowing through the inlet pipe. To remove this section of the visible domain, a filter was added to a spreadsheet document using a straight line found to segment this inlet pipe; which ran from (0,450) to (300,0). Therefore anything under this line is unnecessary.

$$y = -1.5x + 450$$

In the StarBasic programming language (which was utilised throughout the manipulation of these datasets), this is achieved through the command:

$$= IF\left(Y_{ref} \leq \left(\left((-1.5) * X_{ref}\right) + 450\right); 0; 1\right)$$

Since one side of the domain included the inlet pipe; as described above; and the inlet within the test rig itself; which produces very turbulent flow due to a sharp right angle in the pipe, at its end (to direct the flow tangentially, to aid the vortex formation), and also introduces air bubbles which are detected by the PIV system regardless of the positioning of the laser plane, as well as being a solid object disrupting the flow; it was concluded that eliminating the data from that side of the domain would be acceptable and would significantly reduce the number of additional filters that would be required to negate the inlet pipe, and the effects the inlet flow has on the area of the domain surrounding it. As such, with the positioning of the test rig as it was, the simplest method to only give data for one half of the domain was to only allow a single tangent wave to be sampled. This also removes the issue of radial sample lines of a particular angle containing data from two completely opposing positions (one either side of the domain).

$$= IF\left(X_{ref} < 364; 0; 1\right)$$

Which was included in the previous filter to reduce the computation required to remove the

data.

$$= IF\left(Y_{ref} \leq \left(\left((-1.5) * X_{ref}\right) + 450\right); 0\,; IF\left(X_{ref} < 364\,; 0\,; 1\right)\right)$$

The vector values recorded by the PIV system, itself having no scale, are given in px/dt, and so must be converted into a user friendly format, in this case m/s. Since the number of px/m is known, as are details about the camera sampling rate (which are user defined), the conversion factor can be found.

$$\frac{px}{m} = 1742$$

$$\frac{px}{dt} = V_{ref}$$

$$Pulse\ Width,\ pw = 10\,ms = 0.01\,s$$

$$\frac{s}{dt} = \frac{1}{ps} = 100$$

$$\frac{m}{s} = \frac{m}{px} \times \frac{px}{dt} \times \frac{s}{dt}$$

$$\frac{m}{s} = \frac{100}{1742} V_{ref}$$

The angle which the point makes to the reference horizontal line was found and rounded to 0.1 rad precision to provide a larger data sample to give a more comprehensive representation of the flow, this gave approximately 28 data points for every angle grouping. This gave enough data to display the general trend of flow, and highlight outlying data.

$$= ROUND\left(ATAN\left(\left(X_{ref} - 364\right)/\left(Y_{ref} - 260\right)\right); 1\right)$$

The radial position of each coordinate point was then found using basic trigonometry. For the single sample line data, this value was retained at its initial precision, however for the averaged data this value was rounded to 0.01m to provide a simple sampling rate, and to provide 15 data points over the range of the radius. Again this was deemed necessary to provide a large enough data set (an average of 23 points averaged for each radial position).

$$=ROUND\left(\left(\left(\left(X_{ref}-364\right)\text{^}2\right)+\left(\left(Y_{ref}-260\right)\text{^}2\right)\right)\text{^}\left(0.5\right)\right)/1742\,;0.01\right)$$

The tangential velocity of the vector components was found by summing together the Cartesian coordinate components in the tangential direction. For this, an absolute (positive) value was found and this was mated to a radial direction test to remove the components of backflow in the system.

$$=\text{ABS}\left(\left(U_{ref}/\text{SIN}\left(\theta_{ref}\right)\right)+\left(V_{ref}/\text{COS}\left(\theta_{ref}\right)\right)\right)$$

$$=\text{IF}\left(U_{ref}<0\,;0\,;1\right)$$

For the individual angle plots, two sets of graphs were produced for each outlet and at three heights in the flow, one with the mean velocity (with direction left unconsidered), and the other with the tangential velocity, both plotted against the radial position, for each 0.1 rad.

For the averaged data, a sample of ten different recordings of data (therefore spanning a 0.5 second period) was taken, and the values of U and V (velocity in the X and Y direction respectively) were averaged, prior to the analysis listed above. Post the alterations made above, the average tangential velocity over half of the domain (from -1.5 rad to 1.5 rad) was plotted against the radial position. This process is described graphically in Appendix.1.

## *8.2.3 - Results*

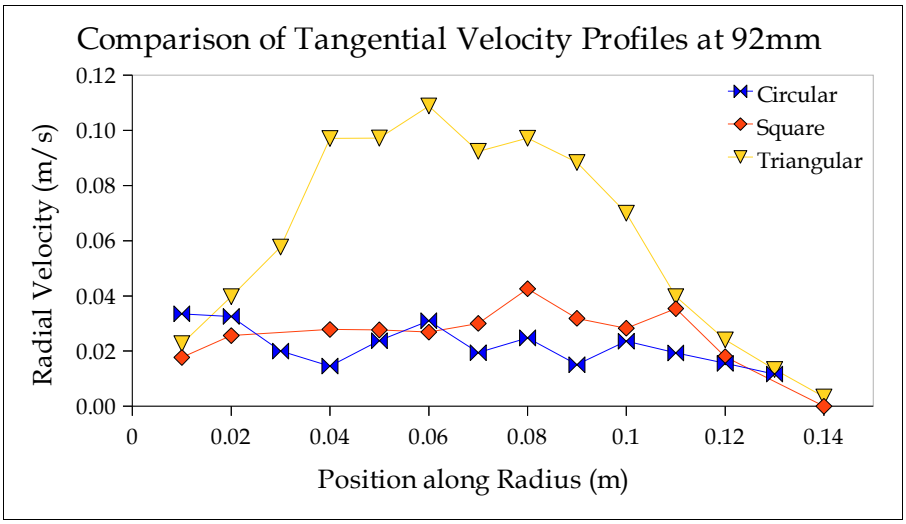


*Fig.17- Low level tangential velocity profiles for various outlets.*

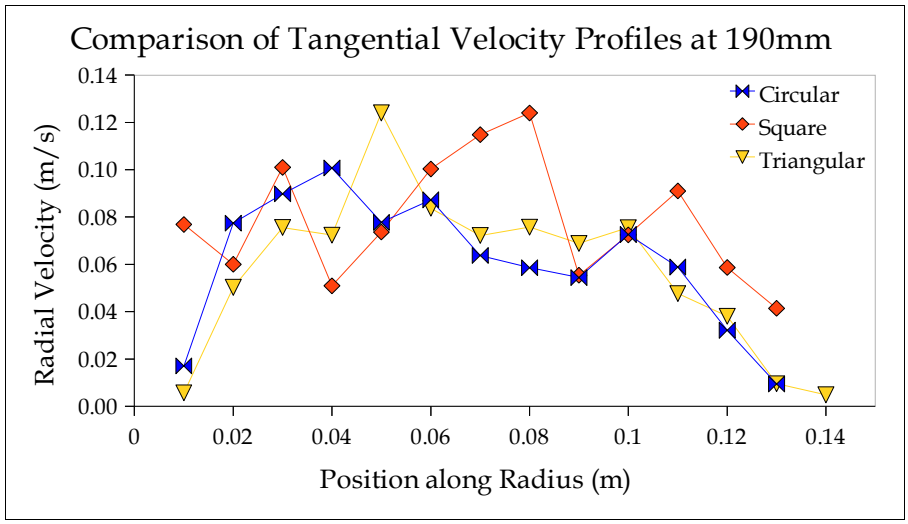


*Fig.18 - Mid level tangential velocity profiles for various outlets.*

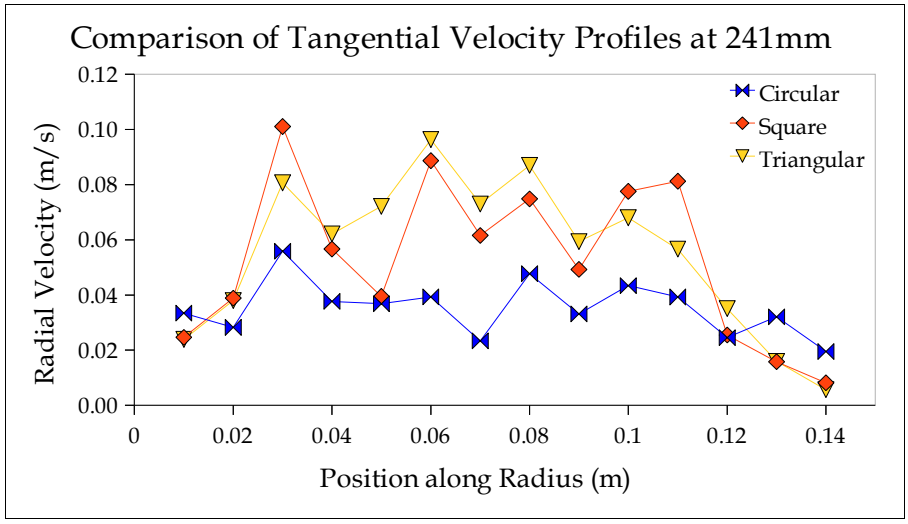


*Fig.19 - High level tangential velocity profiles for various outlets.*

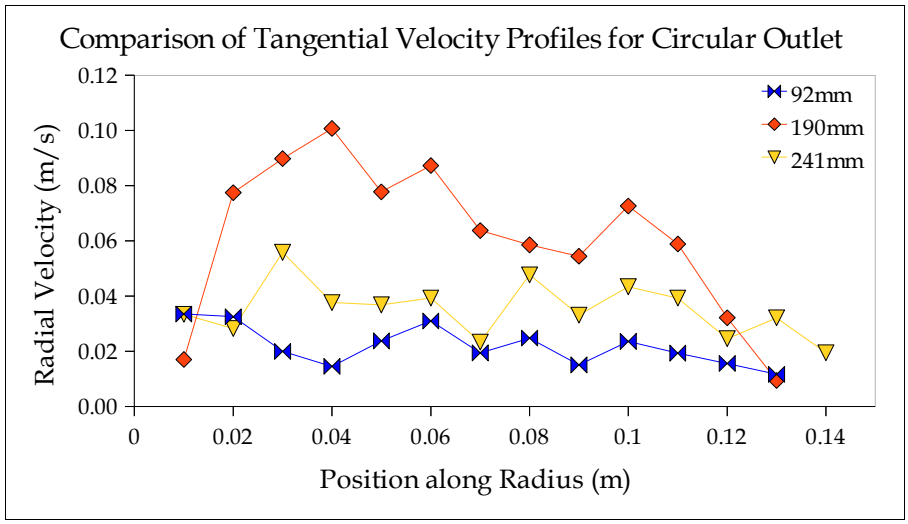


*Fig.20 - Comparison of flow profile variation with height up domain - circle.*

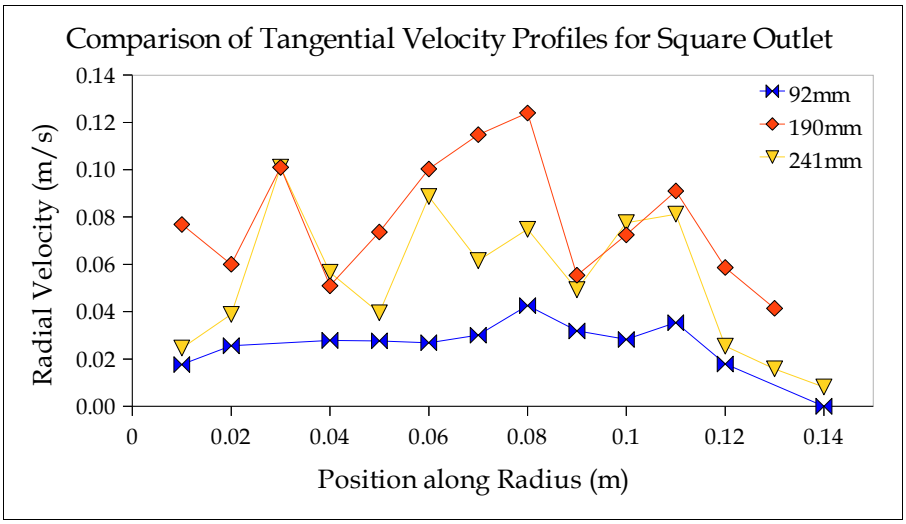


*Fig.21 - Comparison of flow profile variation with height up domain - square.*

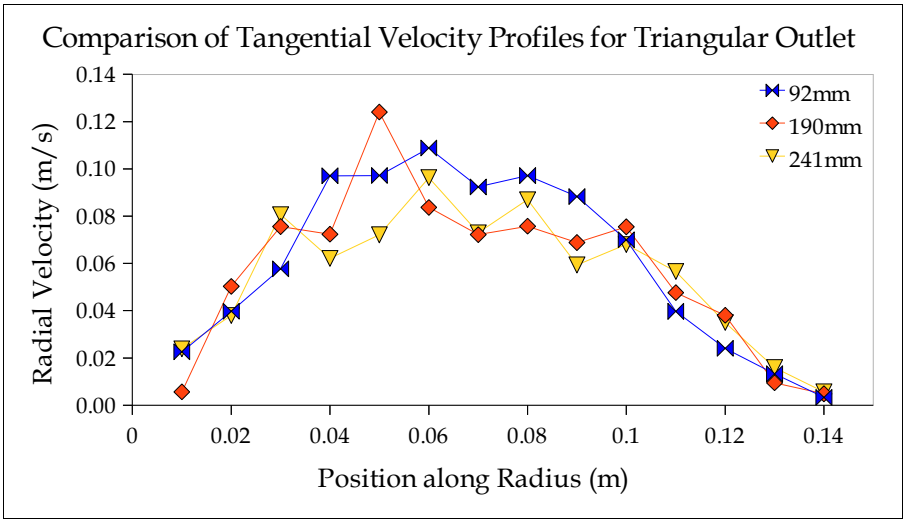


*Fig.22 - Comparison of flow profile variation with height up domain - triangle.*

## *8.2.4 - Analysis*

The three graphs (Fig.17 to Fig.19) display clearly the expected flow velocity profile for the VFC device, with a quadratic profile, having the highest velocity evident over the main flow section (between the edge of the vortex and the wall). Wall effects explain the reduction in tangential velocity at the approach to the edge of the domain (which would be expected to raise according to the vortex strength relationship:

$$\frac{v}{g}\left(\frac{v}{r}+\frac{\delta v}{\delta r}\right)$$

$$\frac{v}{r}+\frac{\delta v}{\delta r}=0$$

*Integrating*

$$\log_e v+\log_e r=Constant$$

Performing this calculation on the velocity data (Appendix.3), produces a constant C of -6.05, with minor variation (an average standard deviation of 0.94 over the entire data set, and 0.3 over the different outlets) seen. When the final two locations are ignored (to ignore the wall effect), the value of C is -5.63, and there is an even smaller variation (an average standard deviation of 0.45 over the entire dataset, and 0.5 over the different outlets).

All three outlets appear to display similar strength coefficients of; 5.99, 5.59 and 5.32 for the circle, square and triangle geometries respectively. This demonstrates the difference in flow velocity attributed to the same inlet conditions, and can be put down almost entirely to the outlet shape.

Comparing the graphical results directly, the triangular outlet appears to demonstrate a higher tangential flow velocity over the entire height of the domain, where the square and circular outlets have a much higher velocity at the 190mm measurement height, concurrent with the pressure tapping results.

## 8.3 - Visual Inspection

Alongside the PIV testing, a number of small visual tests were undertaken on the VFC. The vortex core was monitored over a period of time and images where the main focus was on the core were taken alongside a scaled ruler to determine the air core diameter. This was repeated several times, and the median value taken, which are shown in Tab.2. For the three outlets, the vortex size is similar, and all were of comparable structure (being vertical and with pirouetting only occurring over a confined area of a few millimetres). The measured variation in the vortex core diameter was only noticeable on the triangular outlet, where a much smaller core was present and pirouetting occurred less often and by a lesser distance.

| | Flow Rate (L/s) | Vortex Diameter (m) |
|---|---|---|
| Circle | 0.86 | 0.018 |
| Square | 0.88 | 0.017 |
| Triangle | 0.86 | 0.015 |

*Tab.2 - Vortex core dimension data.*

General inspection of the flow characteristics was also completed and, the main flow region appeared to exist in a large portion of the domain, with a small area at the base and top of the test rig having reduced flow rate. Where dye tracers were introduced through the pressure tapping locations on the side wall, it was noted that the period for fluid to pass through the test rig completely was small, and approximately 3 seconds for the highest flow rates. As the dye appeared to travel in a horizontal plane, the expected vortex characteristics were present, with vertical flow only occurring near the core of the vortex.

# 9 - CFD Comparison

The inlet conditions for the computational model differ significantly from that of the physical. A physical inlet pipe is used in the experimental rig, which introduces fluid into the main flow region, where the computational model has an inlet situated at the wall, and therefore no intrusive pipe to disrupt the flow of the fluid (where significant cavitation is seen after the inlet pipe on the test rig). It must however introduce fluid at an angle which differs from the main flow, since it is angled and aligned to introduce fluid at the same angle as the experimental set up, at the same point, yet exists away from this point.

Comparing the wall pressure measurements for various flow rates for the circular (control) outlet (Fig.23), some significant variation can be seen between the two methods of data gathering. The experimental method provides a clear pressure profile, with a maximum value being seen towards the mid height of the test rig, and having a variation of 1% over the recorded height of 180mm, whereas the computational results show higher pressures evident

at the base, and at the top of the flow, with a constant pressure throughout the main flow region.

It was not available using the experimental test rig to obtain pressure readings for positions close to the base or top of the test rig, and therefore the effect of the different flow situations in these areas remains unseen, however it should be concluded that, considering the variation in pressure given by the experimental method is just 1%, and the general pattern; that the gauge pressure increases with an increased flow rate; is upheld by both methods, the computational results are representative of the true flow within the test rig. The computationally recorded pressures for the high flow rates (1.26L/s) are considerably higher than the experimental values, and are considered significantly erroneous, where the lower flow rates are of similar magnitudes in both cases, and for both outlets. Appendix.5 and .6 display the high flow rate data alongside the more concurring data.

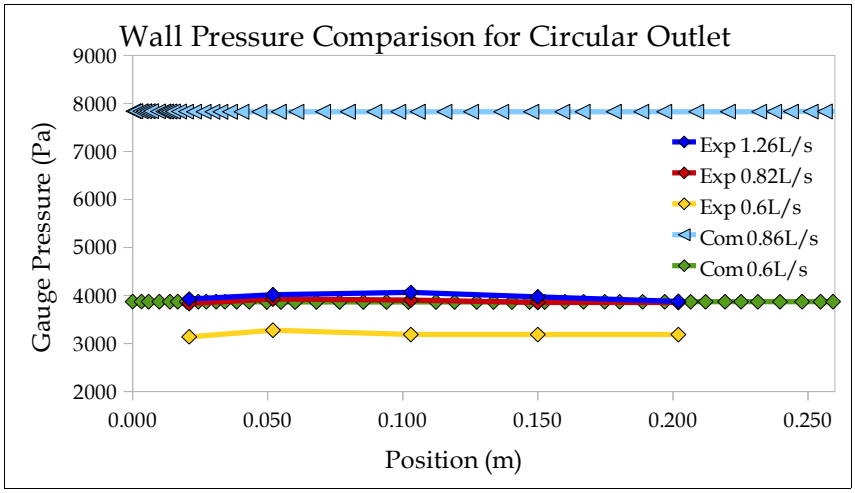


*Fig.23 - Circular outlet pressure comparison: Experimental vs. Computational.*

The triangular outlet comparison graph (Fig.24) displays similar pressure values being obtained for relative flow rates between the experimental and computational models. Again there is a difference in pressure profile; where in the case of the triangular outlet, the wall effects at the base and top are not seen and a very stable pressure is recorded over the height of the domain, and the experimental results still display the quadratic relationship, with pressure highest at the mid point of the main flow region.

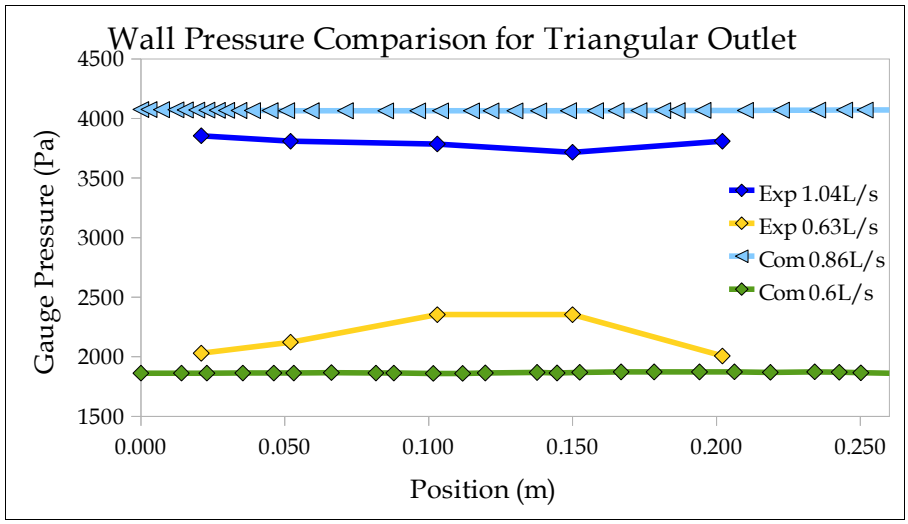


*Fig.24 - Triangular outlet pressure comparison: Experimental vs. Computational.*

The results obtained for the tangential velocities along a radial line from the centre of the flow were at least a factor of 10 different, with the computational simulation producing results of over 1 m/s towards the centre of the flow, and the experimental test rig rarely giving averaged results above 0.1 m/s (although as seen, the raw data can produce flow velocities nearer 0.9 m/s). The root cause of this inconsistency in data remains unknown at present, however a significant contributing factor may lie in the PIV systems inability to detect the flow of the vortex core. This area of flow is very rapid relative to other areas, and the variation in velocity demonstrated by the computational results would dictate a huge velocity range over a very short sampled distance:

*0.525m/s change in 0.011m with 2126px/m*

*0.525m/s change over 3 data points, or 0.175m/s px*

If this inconsistency is negated however, and the computational velocity profile is only compared within the main flow region, then the same general characteristics can be observed, with a slowly increasing flow velocity: relating to the vortex strength relationship, which is similar for both experimental and computational. If the wall effect area is estimated to exist 0.02m into the main flow (as demonstrated by the computational model), then a small area of the flow, between 0.02m and 0.04m away from the wall, can be considered anomalous under experimental data capture methods. This may be due to the construction of the test rig (where significant portions of silicone were present in small areas overlapping the

flow, and so particular areas of flow were not captured by the PIV system), and through the averaging of the data over half of the domain, where the higher expected results may have been sampled out of the final dataset. When individual time point data sets are considered, a large number of previously considered, erroneous data, can be seen in the outer regions of the flow, which are not seen in the averaged data.

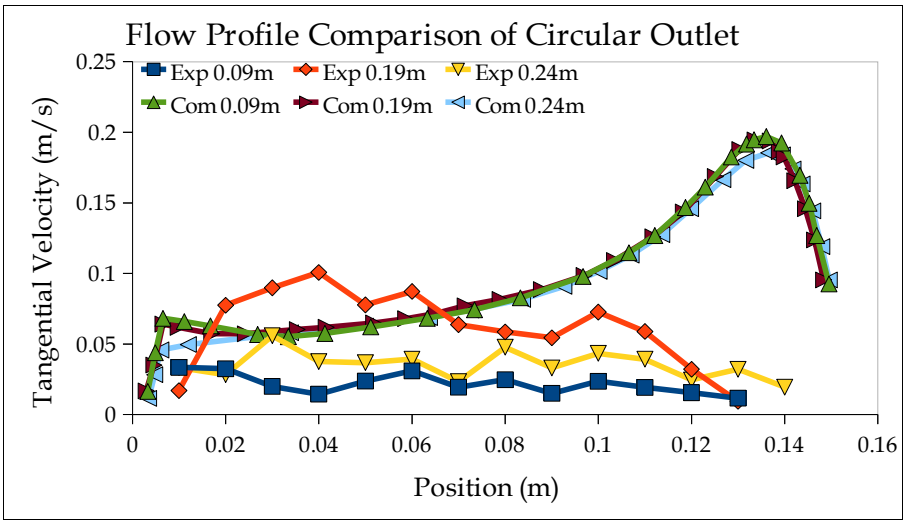


*Fig.25 - Comparison of flow velocity profiles for a circular outlet at 0.86 L/s.*

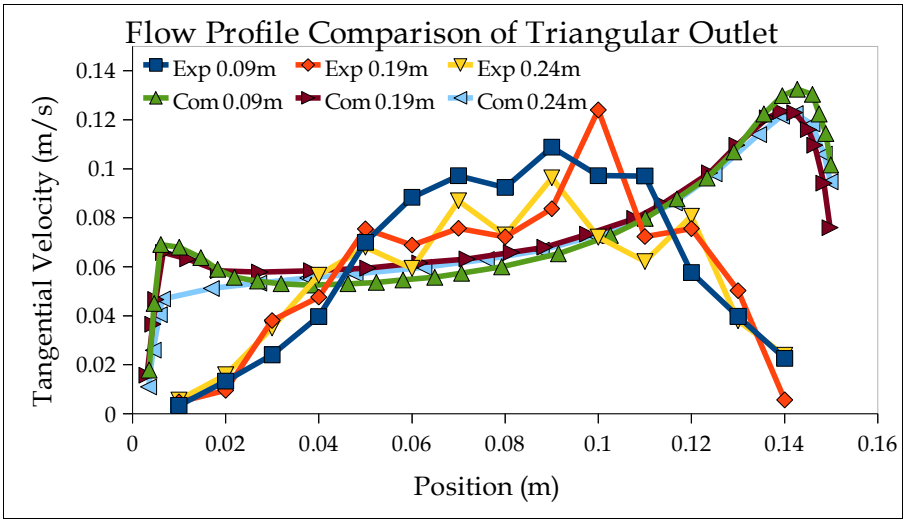


*Fig.26 - Comparison of flow velocity profiles for a triangular outlet at 0.86 L/s.*

Figures .25 and .26 display the experimentally recorded data, and the computational data with a factor of 0.1 included, the true data sets (which are not comparable) are shown in appendix.7 and .8.

# 10 - Conclusions

The experimental test rig utilised in this investigation, allowed a direct comparison of the flow regimes present for three different outlets, and it is evident that the outlet geometry can significantly affect the vortex flow under high flow rate conditions. The vortex strength is highest with the circular outlet, which leads to higher velocities at the vortex core (demonstrated by the CFD analysis) and lower velocities in the main flow: a point backed up by the velocity measurements of the triangular outlet which has the highest main flow velocity, the highest main flow pressure, and the lowest vortex strength.

The vortices of the three outlets appear to follow the expected flow relationships, with the pressure being related to the tangential velocity (which is expected to be the main component of flow), and the velocities being related to the radial distance for a given circumstantial vortex strength.

The computational comparison displays the shortcomings of the PIV system and the manual pressure recording, however the exclusion of the vortex core and the wall effect areas produces comparable flow characteristics, despite the significant difference in raw values for pressure and velocity between the two.

Future work should be undertaken to determine the cause of the large variation in pressure difference seen in the CFD simulation under high flow rates, and a study on the flow at the core of the vortex would be valuable in determining the physical relationships between the outlet geometry and the vortex structure. These two undertakings should be completed prior to computational studies being the primary source of geometry testing of VFC devices.

# 11 - Evaluation

Several significant inaccuracies were highlighted in the undertaking of this project. With the test rig design itself, the inclusion of a physical inlet pipe into the main flow produced significant turbulence for the rotating fluid, and resulted in a significant portion of the domain being unsuitable for data capture. The use of a more precise pressure measurement technique: such as a series of piezoresistive sensors, would also be highly beneficial to discover the precise velocity variations over the base and top of the vortex (where the highest radial flow is evident).

The PIV system would be more suited to measurement of smaller areas of flow, since the low sample rate results in the areas of high velocity gradient being overly simplified, and therefore not satisfying the neighbour average rules utilised by the software to determine velocities (commonly a root mean squared derived rule). However, the light levels required to perform the testing were not as low as expected. For the start of testing, a camera light meter at the test rig height measured a light level of 0.48 lux, with the camera being exposed to a higher light level due in part to its height relative to the light shield, and this produced results with a high particle numbers, both with and without the use of aluminium tracer particles.

The pirouetting of the vortex core, although small, does results in a variable radius being evident within the domain, which is unaccounted for in the PIV analysis, however the computational requirements of recording and saving an image every frame, and the manual input required in interpreting the location of the vortex axis, is significant and would not remove any significant error in the radial sampling due to the 0.01m sample rate used throughout this project.

# 12 - Appendix

*Appendix.1 - Flow diagram displaying the data manipulation process.*

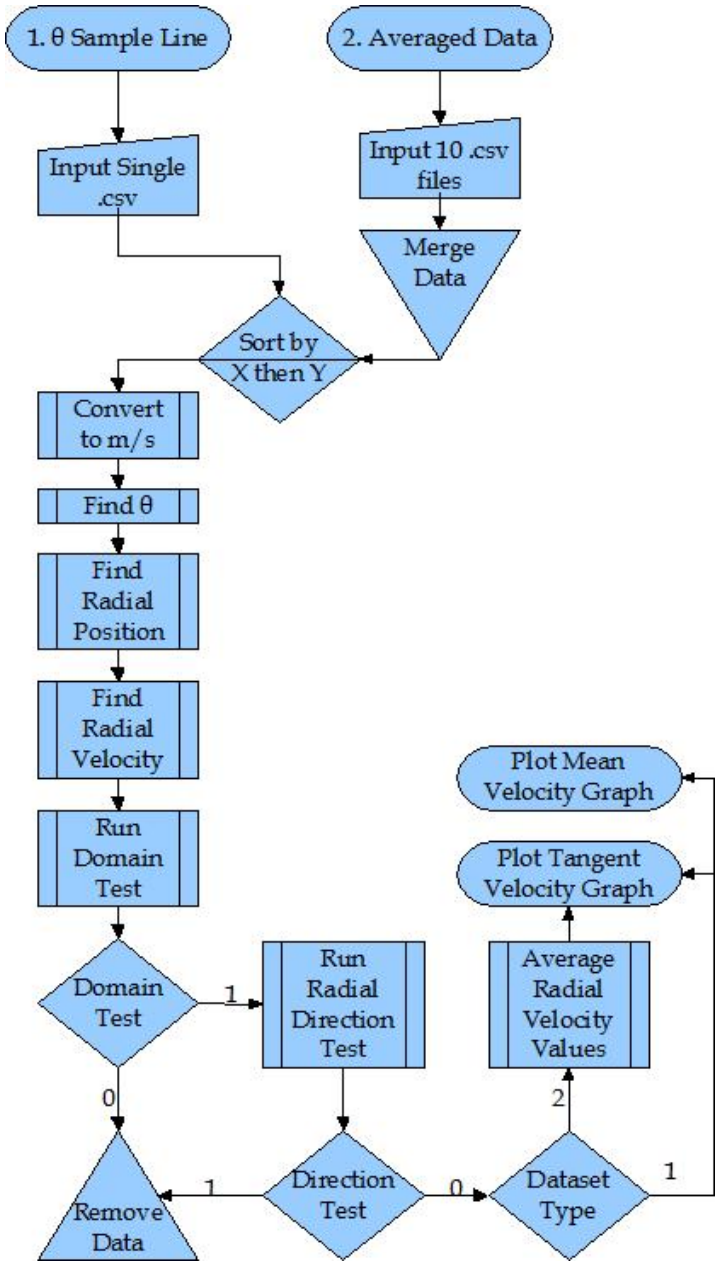

*Appendix.2 - Vortex strength and deviation numerical data.*

| Outlet Type | Measurement Position (mm) | Vortex Strength | Resampled Vortex Strength | Standard Deviation |
|---|---|---|---|---|
| Circle | 92 | -6.74 | -6.61 | 0.52 |
| | 190 | -5.82 | -5.37 | 0.29 |
| | 241 | -6.19 | -5.99 | 0.43 |
| Square | 92 | -6.48 | -6.12 | 0.45 |
| | 190 | -5.47 | -5.22 | 0.55 |
| | 241 | -5.94 | -5.43 | 0.52 |
| Triangle | 92 | -5.91 | -5.27 | 0.48 |
| | 190 | -6 | -5.33 | 0.39 |
| | 241 | -5.9 | -5.37 | 0.41 |
| **Average** | | **-6.05** | **-5.63** | **0.45** |

*Appendix.3 - Numerical results of averaged velocity data.*

| Outlet Type | Measurement Position (mm) | Maximum Averaged Tangential Velocity (m/s) | Maximum Averaged Grouped Tangential Velocity (m/s) |
|---|---|---|---|
| Circle | 92 | 0.224 | 0.033 |
| | 190 | 0.688 | 0.101 |
| | 241 | 0.583 | 0.056 |
| Square | 92 | 0.163 | 0.043 |
| | 190 | 0.777 | 0.101 |
| | 241 | 0.739 | 0.124 |
| Triangle | 92 | 0.883 | 0.109 |
| | 190 | 0.878 | 0.124 |
| | 241 | 0.571 | 0.096 |
| Maximum | | **0.883** | **0.124** |

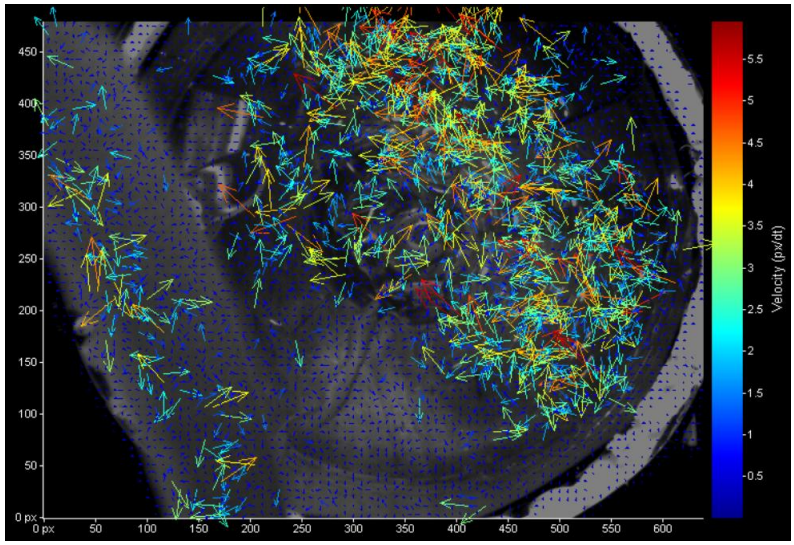


*Appendix.4 - Sample PIV vector image.*

Appendix II

*Appendix.5 - Full circular pressure comparison: Experimental vs. Computational.*

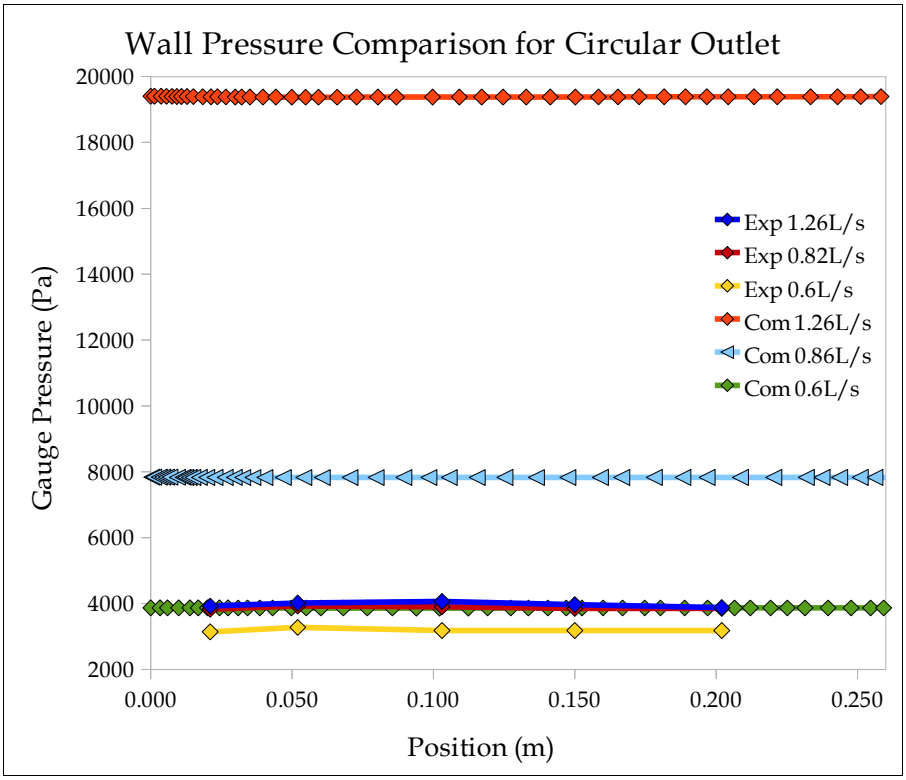


*Appendix.6 - Full triangular pressure comparison: Experimental vs. Computational.*

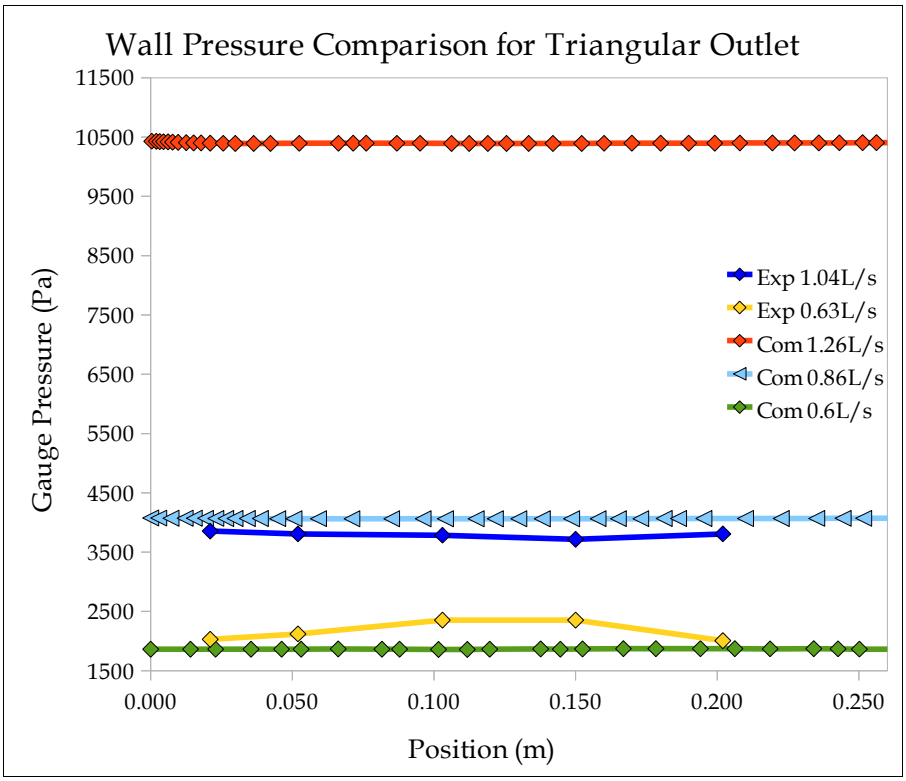

*Appendix.7 - Full comparison of velocity profiles for circular outlet at 0.86 L/s.*

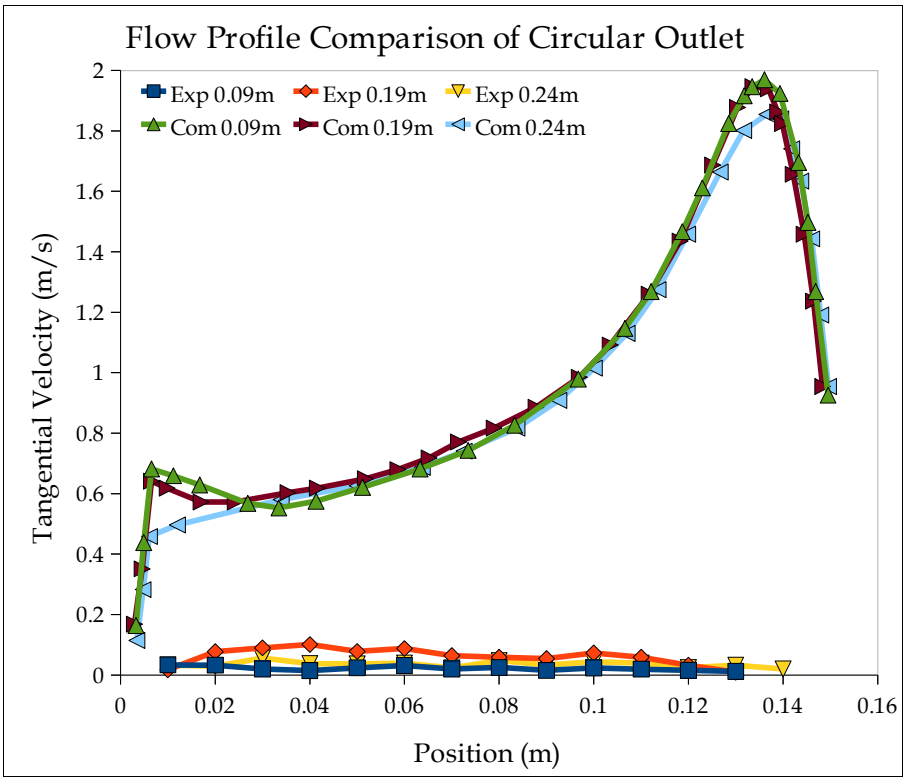


*Appendix.8 - Full comparison of velocity profiles for triangular outlet at 0.86 L/s.*

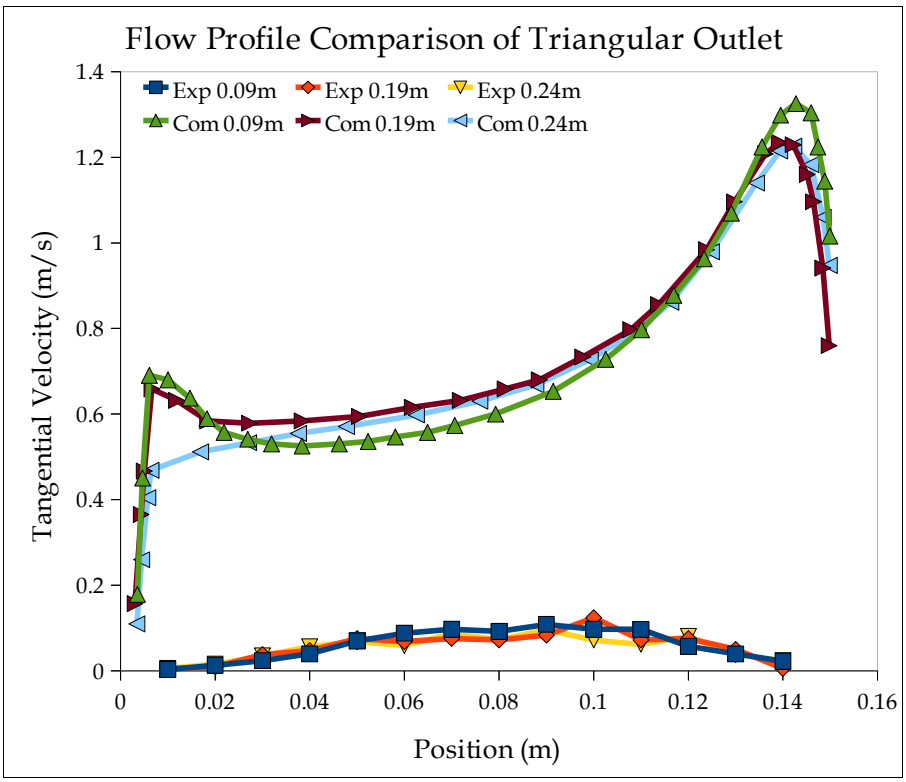

# 13 - Bibliography


1. Venn, R. Worrall, E. Engel, B. et al., (2011) Evolutions in vortex flow control.

2. Newton, C. (2011) Design and Construction of Vortex Rig.

3. Jarman, D. (2011) A Study of the Design of Cylindrical Vortex Flow Controls for use in Urban Drainage Systems.

4. Williams, N. (2011) An Investigation into the CFD Modelling of Forced and Confined Vortices with varied Outlet Geometry.

5. Ackers, P. White, W. Perkins, J. Harrison, A. (1978) Weirs and Flumes for Flow Measurement, New York, Wiley.

6. Douglas, J. Gasiorek, J. Swaffield, J. (2001) Fluid Mechanics, 4th ed. Harlow, Pearson Education.

7. Asawa, G. (2006) Laboratory Work in Hydraulic Engineering, New Delhi, New Age International.

8. Akshoy, R. Sanchayan, M. Pijush, R. (2005) Mechanical Sciences: Engineering - Thermodynamics and Fluid Dynamics, New Delhi, Prentice Hall.

9. Durst, F. (2008) Fluid Mechanics – An Introduction to the Theory of Fluid Flows, Berlin, Springer.

10. Yamaguchi, H. (2008) Engineering Fluid Mechanics, Dordrecht Netherlands, Springer.

11. Subramanya, K. (2008) Engineering Hydrology, 3rd ed. New Delhi, Tata McGraw-Hill.

12. Graebel, W. (2001) Engineering Fluid Mechanics, London, Taylor & Francis.

13. Sellin, R. (1970) Flow in Channels, New York, Gordon & Breach.